

Structural Studies of Perfluoroaryldiselenadiazolyl Radicals: Insights into Dithiadiazolyl Chemistry

Rebecca L. Melen,^{*,†,‡} Robert J. Less,[†] Christopher M. Pask,[†] and Jeremy M. Rawson^{*,†,§}

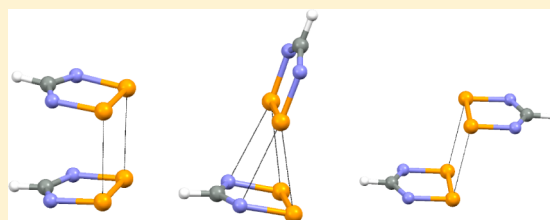
[†]Department of Chemistry, University of Cambridge, Lensfield Road, Cambridge CB2 1EW, U.K.

[‡]School of Chemistry, Cardiff University, Main Building, Cardiff, CF10 3AT Cymru/Wales, U.K.

[§]Department of Chemistry and Biochemistry, University of Windsor, 401 Sunset Avenue, Windsor, Ontario N9B 3P4, Canada

S Supporting Information

ABSTRACT: The synthesis and structural characterization of a series of perfluoroaryldiselenadiazolyls [DSeDA; p -XC₆F₄CNSeSeN (X = F, Cl, Br, CF₃, NO₂, and CN for **2a–2f**, respectively)] are described. Concentration-dependent solution UV/vis measurements on **2a** follow the Beer–Lambert law and the transitions assigned through time-dependent density functional theory (TD-DFT) studies, indicating little propensity for dimerization in solution (10^{-3} – 10^{-4} M). Solution electron paramagnetic resonance (EPR) spectra reveal that these radicals exhibit a broad featureless singlet around $g = 2.04$ but form well-resolved anisotropic EPR spectra in frozen solution, from which spin densities were determined and found to reflect an increase in the spin density at the chalcogen in relation to the corresponding dithiadiazolyl (DTDA) radicals, p -XC₆F₄CNSSN. The solid-state structures of **2a** and **2d–2f** all adopt spin-paired cis-cofacial dimers in which the dimers are held together via multicenter $\pi^*-\pi^*$ “pancake bonding” interactions. Conversely, **2b** and **2c** exhibit an orthogonal mode of association, which is unique to DSeDA chemistry but which also affords a singlet ground state evidenced by SQUID magnetometry. The more sterically demanding diselenadiazolyl radical **2f** was also prepared and exhibits a trans-antarafacial dimerization mode. DFT studies [UPBE0-D3 ccPVTZ-PP(-F)++] on the model radical HCNSeSeN confirm that each dimer is a stable energy minimum on the potential energy surface, reproducing well the experimental geometric parameters with relative stability in the order cis-cofacial > orthogonal > trans-antarafacial. Computational studies reflect stronger dimerization for DSeDA radicals in relation to their sulfur analogues, consistent with the experimental observation: While **2a** and **2d** are isomorphous with their corresponding DTDA radicals, **2b**, **2c**, and **2e–2g** are all dimeric, in contrast to their DTDA analogues, which are monomeric in the solid-state. A study on **2f** reveals that significant geometric strain accumulates in order to support the propensity for both cis dimerization and intermolecular CN \cdots Se interactions. Conversely, p -NCC₆F₄CNSSN likely forfeits dimerization in the analogous packing motif in order to release strain but retains the favorable intermolecular CN \cdots S interactions.



INTRODUCTION

The magnetic^{1,2} and transport³ properties of dithiadiazolyl (DTDA) radicals have attracted considerable attention since the first structural report of a DTDA radical, [PhCNSSN]₂, in 1980.⁴ More recently, their coordination chemistry as paramagnetic ligands in molecule-based magnetic materials has been exploited by Preuss,⁵ and approaches to control their solid-state structure through crystal engineering design strategies have been reviewed by Haynes.⁶ In the majority of cases, these DTDA radicals adopt dimeric structures with short intradimer S \cdots S contacts (ca. 3.0 Å), which are significantly less than the sum of the van der Waals radii (3.6 Å) but more than a covalent S–S bond (2.0 Å). Structural studies on these DTDA dimers reflect a range of dimerization modes (cis, twisted, trans etc.) in which there is a strong orientational preference, supporting the hypothesis that dimerization is associated with a bonding interaction between the two singly occupied molecular orbitals of a₂ symmetry. The nature of the structure and bonding within these dimers continues to be a point of discussion. Initial descriptions by Banister and Gillespie favored

a 4-center, 2-electron bonding interaction between the S atoms,^{4,7} whereas Gleiter et al. utilized variously a 4-center, 6-electron dimer or 14-electron σ/π -delocalized dimer description.⁸ Recent charge-density studies by Haynes et al. showed clear electron densities (0.86–0.92 e Å⁻³) at the S–S bond critical point, typical of a conventional covalent bond, but much lower electron densities at the intradimer S \cdots S bond critical points (0.14–0.17 e Å⁻³), consistent with a delocalized multicenter bonding interaction.⁹ More recent magnetic and electron paramagnetic resonance (EPR) studies by Passmore, Rawson, and their co-workers have revealed that many of these dimers exhibit the onset of paramagnetism near room temperature due to the population of a thermally accessible triplet state.^{10,11} This casts some speculation over the nature of the ground-state electronic configuration as to whether it is a closed-shell “spin-paired” singlet, an open-shell “antiferromagnetically coupled” singlet, or an admixture of these two

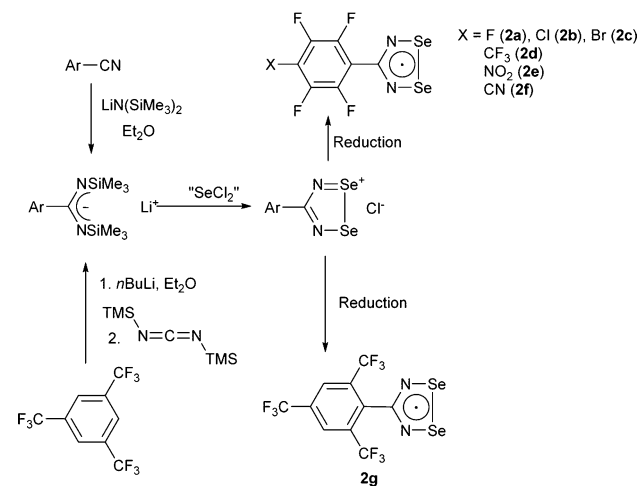
Received: July 27, 2016

Published: November 1, 2016

possibilities. Computational studies suggest that the ground state has ca. 30% diradical character.¹² These DTDA radicals comprise one member of a larger family of so-called “pancake dimers” in which the intermolecular contacts are much stronger than conventional van der Waals contacts and display a strong orientational dependence consistent with some degree of orbital interaction.¹³

The replacement of sulfur by selenium has several possible attractions. In the context of transport properties, Oakley et al. have shown that the replacement of sulfur by selenium often leads to isomorphous materials, with the selenium derivatives offering superior electron-transport properties due to the more radially diffuse nature of the 4p orbitals.¹⁴ Conversely, the development of selenium analogues of DTDA radicals as building blocks for organic magnetic materials has not been examined. In related thiazyl and selenazyl radical systems, the substitution of sulfur by selenium has led to stronger magnetic exchange coupling through the more diffuse nature of the 4p valence orbitals of selenium as well as a larger magnetic anisotropy,¹⁵ which scales as Z^4 .¹⁶ In this context, the preparation and characterization of heavier p-block analogues of paramagnetic DTDA radicals appeared attractive, particularly given the seeming propensity for DSeDA radicals to adopt similar or isomorphous packing to their DTDA analogues.¹⁴ As an extension of our previous studies on perfluoroaryl and sterically encumbered DTDA radicals,^{1,2,17} we now describe the preparation and structural characterization of their heavier diselenadiazolyl, DSeDA, congeners, *p*-XC₆F₄CNSeSeN (X = F, Cl, Br, CF₃, NO₂, and CN for **2a–2f**, respectively) and 2,4,6-(F₃C)₃C₆F₂CNSeSeN (**2g**; Scheme 1).

Scheme 1. General Synthetic Route to Novel Diselenadiazolyls **2a–2g**



RESULTS AND DISCUSSION

The synthesis of the diselenadiazolyl radicals **2a–2f** followed a method similar to that used to prepare the related DTDA radicals using a mixture of SeCl₄ and elemental selenium as a source of SeCl₂ (Scheme 1).¹⁸ This source of SeCl₂ is preferred over a 1:1 mixture of Ph₃Sb and SeCl₄, which, in our hands, has, on occasion, been violently exothermic when mixed together in the solid state. Reduction of the sparingly soluble chloride salt [**2**]Cl was readily achieved via one-electron reduction in a polar solvent. Assorted reducing agents (silver powder, Zn/Cu couple, or Ph₃Sb) in a range of polar solvents [acetonitrile

(MeCN), tetrahydrofuran (THF), or liquid SO₂) proved successful in driving the one-electron reduction, evidenced by the color change to deep purple and the appearance of an EPR signal. However, separation of the radical from the solvent and byproducts proved problematic. The use of silver powder in THF proved successful for both **2b** and **2e** but, in other cases, formed oily residues from which pure radical could not be isolated by sublimation. The use of Ph₃Sb in MeCN as an alternative reductant can be successfully (**2a**, **2c**, and **2f**) used provided the radical does not sublime at temperatures similar to those of Ph₃Sb (mp 52–54 °C), which can contaminate the sample or lead to cocrystallization.¹⁹ For volatile radicals or those with a high solvent affinity, the use of Zn/Cu couple in highly volatile liquid SO₂ proved successful (**2d** and **2g**).

Radical **2g** was prepared using a method analogous to the preparation of the sulfur analogue.^{17c} The crude diselenadiazolyl radicals (**2a–2g**) were purified by vacuum sublimation in glass tubes with crystals of **2a–2g** grown by vacuum sublimation under static vacuum (10⁻¹ Torr). Yields were not optimized for these predominantly structural studies but were up to 54% recovered yield based on the starting material.

Solution Studies on **2.** Unlike DTDA radicals, which exhibit well-resolved solution EPR spectra ($g = 2.01$ and $a_N \sim 5.0$ G), the EPR spectra of **2** in THF were observed as broad singlets at $g = 2.04$ (see the Supporting Information, SI). Similar spectra were observed at low concentration, indicating that this was not due to dipolar broadening effects but was the result of significant g -tensor anisotropy (vide infra), consistent with previous observations.^{18,20} However, frozen-solution spectra provided well-resolved features reflecting rhombic symmetry, and the frozen-solution EPR spectrum of **2b** is shown in Figure 1. The EPR spectrum reveals well-resolved hyperfine coupling to two ¹⁴N nuclei of the g_{xx} component of the spectrum, and ⁷⁷Se satellites for both g_{xx} and g_{zz} were directly observed with estimates of additional hyperfine couplings based on the fit to the EPR profile. These parameters are compared with those of C₆F₅CNSeN²¹ in Table 1. The

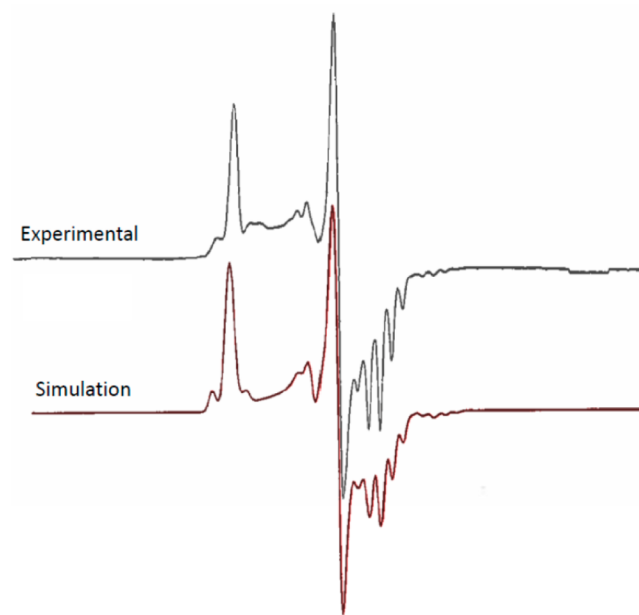


Figure 1. Frozen-solution EPR spectrum of **2b** in THF at 77 K. Simulation parameters are given in Table 1.

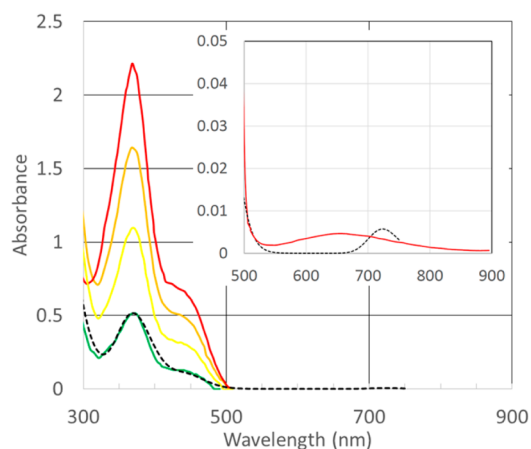
Table 1. EPR Simulation Parameters for **2b** (Line Width = 3.2 G_{pp}) and for C₆F₅CN₂SSN²¹

parameter	g_{xx}	g_{yy}	g_{zz}	$\langle g \rangle$	g_{iso}
2b	1.9828	2.0214	2.1001	2.0346	2.0376
C ₆ F ₅ CN ₂ SSN	2.0025	2.0085	2.0220	2.0110	2.0102
parameter	$A(N) + A_{xx}(N)/G$	$A(N) + A_{yy}(N)/G$	$A(N) + A_{zz}(N)/G$	$\langle a(N) \rangle / G$	$a(N) / G$
2b	13.67	2.00	1.33	5.67	
C ₆ F ₅ CN ₂ SSN	13.84	1.00	0.31	5.05	5.17
parameter	$A(Se) + A_{xx}(Se)/G$	$A(Se) + A_{yy}(Se)/G$	$A(Se) + A_{zz}(Se)/G$	$\langle a(Se) \rangle / G$	$a(Se) / G$
2b	130.66	-56.00	-3.87	23.6	

absolute signs of the ⁷⁷Se hyperfine interactions are not known, but the two smaller ⁷⁷Se hyperfine couplings were considered opposite in sign to the largest coupling because ⁷⁷Se satellites beyond the line width of the isotropic EPR spectrum were not observed, consistent with previous reports on the isolobal S₃N₂^{•+} and Se₂N₂S^{•+} radical cations.²⁰ These spectral parameters were common across several derivatives of **2**. An estimate of the spin-density distribution in these DSeDA radicals can be made based on the EPR parameters and has proved successful in assessing the spin density in other thiazyl and selenazyl radicals.²⁰ In the case of DTDA radicals, estimates of the spin-density distribution from EPR have been in very good agreement with measured spin densities determined from polarized neutron diffraction studies as well as density functional theory (DFT) calculations.²² These calculations (see the SI) provide total spin densities of 21% and 31% on the N and Se atoms, respectively (see the SI). Thus, replacement of sulfur by selenium leads to a small reduction in the spin density at N and an increase at the chalcogen in relation to DTDA radicals, a trend that has been previously observed for S₃N₂^{•+} and its selenium derivatives.²⁰ A comparison of the spin densities from EPR and those from unrestricted DFT studies [PBE0-D3 cc-PVTZ-PP(-F)++] is presented in the SI.

Previous EPR studies on DTDA radicals revealed a monomer–dimer equilibrium in solution with $\Delta H_{dim} \sim 35$ kJ mol⁻¹ for a range of substituents.²³ Additional solution UV/vis studies by Preuss indicated that at concentrations below 10⁻³ M the contributions from the dimer were negligible.²⁴ The increased spin density at selenium appears to lead to greater dimerization in solution reflected in (i) many UV/vis transitions on PhCNSeSeN in THF exhibiting an absorbance that is proportional to the square of the concentration, at concentrations similar to those of the DTDA studies and (ii) an approximately estimated 70% dissociation by EPR.²⁵

In order to examine the effect of the perfluoroaryl group on the monomer–dimer equilibrium, variable-concentration UV/vis studies on **2a** were undertaken in THF in the range 10⁻³–10⁻⁴ M. The visible spectrum is dominated by a well-defined maximum at 369 nm with a shoulder at 433 nm in THF (Figure 2). These transitions exhibit a linear relationship between the absorbance and concentration (see the SI), indicating that these bands are associated with monomeric **2a** in solution. In addition, time-dependent DFT (TD-DFT) calculations [UPBE0-D3 cc-PVTZ-PP(-F)++] on monomeric **2a** replicate very well the salient intense features of the UV/vis data. Similar linear behavior would be observed if the monomer–dimer ratio did not change significantly over the concentration range studied. However, the good agreement between the observed and calculated UV/vis spectra coupled with previous

**Figure 2.** Solution UV/vis spectra of **2a** in THF (2.5×10^{-4} , 5.0×10^{-4} , 7.5×10^{-4} , and 1.0×10^{-3} M) with a calculated absorption profile (---). Inset: Detail of the low-energy region of the UV/vis spectrum with a calculated absorption profile (—).

quantitative EPR studies on [PhCNSeSeN]₂, which revealed at least 70% dissociation in solution,²⁵ suggests that the solution UV/vis spectra are predominantly those of the monomer.

A very weak low-energy absorption at 650 nm is observed at high THF concentrations (10⁻³ M; Figure 2, inset). The broadness and low intensity of this transition inhibited a full analysis of its concentration dependence to distinguish between **2a** and (**2a**)₂. However, the TD-DFT studies on **2a** reveal a weak transition around 720 nm that is associated with the promotion of the unpaired electron from the π^* molecular orbital of a₂ symmetry to the Se–Se σ^* orbital, although we recognize that this does not preclude the broad transition also having a component arising from dimeric (**2a**)₂.

Structural Studies. A summary of the crystallographic data for **2a**–**2g** is presented in the SI, and selected structural data are presented in Table 2.

Crystal Structures of (C₆F₅CNSeSeN)₂ (2a**), (p-F₃CC₆F₄CNSeSeN)₂ (**2d**), (p-O₂NC₆F₄CNSeSeN)₂ (**2e**), and (p-NCC₆F₄CNSeSeN)₂ (**2f**).** All four of these radicals exhibit cis-cofacial dimers (Figure 3). The intradimer Se...Se contacts (Table 2) fall in the range 3.195(5)–3.275(5) Å and are comparable with those of other cis-oid DSeDA derivatives (3.17–3.37 Å; mean 3.26 Å).²⁶ The twist angles between perfluoroaryl and DSeDA rings (θ) fall in the range 34.6–42.0°, comparable with those reported for perfluoroaryl DTDA radicals in which a shallow energy minimum has been computed around 50° with angles in the range 20–90° all within 5 kJ mol⁻¹.²⁷ The angle formed between the two DSeDA ring planes (ϕ) spans a narrow range of 9.0–11.8°, and a degree of strain is observed through bending of the DSeDA ring from the phenylene plane to optimize the close approach of DSeDA rings in the dimer formation. A molecular bowing parameter (β ; defined as the angle formed between the para substituent, the phenylene ring centroid, and the C atom of the DSeDA ring) is used to provide a measure of the total molecular distortion of the substituent and the DSeDA ring from the phenylene ring plane. Deviations from 180° reflect some distortion of the molecular structure. Structures **2a** and **2d**–**2f** provide parameters in the range 173–178°, with cyano and nitro derivatives (**2e** and **2f**) exhibiting the largest distortions from 180°, suggesting a build-up of ring strain.

Table 2. Intradimer Se...Se and Interdimer Se...N Contacts, Torsion Angles (θ) between DSeDA and the Aryl Ring Planes, Inclinations (ϕ) of DSeDA Ring Planes with Respect to Each Other, and Bowing Angles (β) Defined as the Angle Made between the R Group, the Centroid of the Phenylene Ring, and the DSeDA Ring C Atom

compound	intradimer Se...Se/Å	intradimer Se...N/Å	θ /deg	ϕ /deg	β /deg	interdimer Se...N/Å
Cisoid Dimers						
2a (X = F)	3.197(2)		38.8	9.68	176.95	3.092(6) 3.097(6)
2d (X = CF ₃)	3.200(1) 3.208(1)		40.45 42.03	11.83	177.35 177.61	2.941(7) 2.988(7)
2e (X = NO ₂)	3.195(5) 3.275(5)		34.65 40.67	10.68	173.55 176.90	3.06(3) 3.26(3)
2f (X = CN)	3.212(2) 3.220(2)		36.70 36.78	8.96	175.52 175.58	3.14(1) 3.19(1)
Orthogonal Dimers						
2b (X = Cl)	3.110(7) 3.207(7)	3.04(3) 3.11(3)	58.23 59.70	81.51	177.37 177.29	3.06(3) 3.25(3)
2c (X = Br)	3.115(6) 3.187(6)	3.04(3) 3.06(3)	56.34 59.01	84.36	177.80 179.02	3.02(2) 3.22(2)
Trans-Antarafacial Dimer						
2g	3.230(2) 3.316(1) 3.334(2)		75.83 79.01 89.70	7.59 0.00	177.65 178.74 179.26	2.840(9) 3.254(8) 3.288(9)

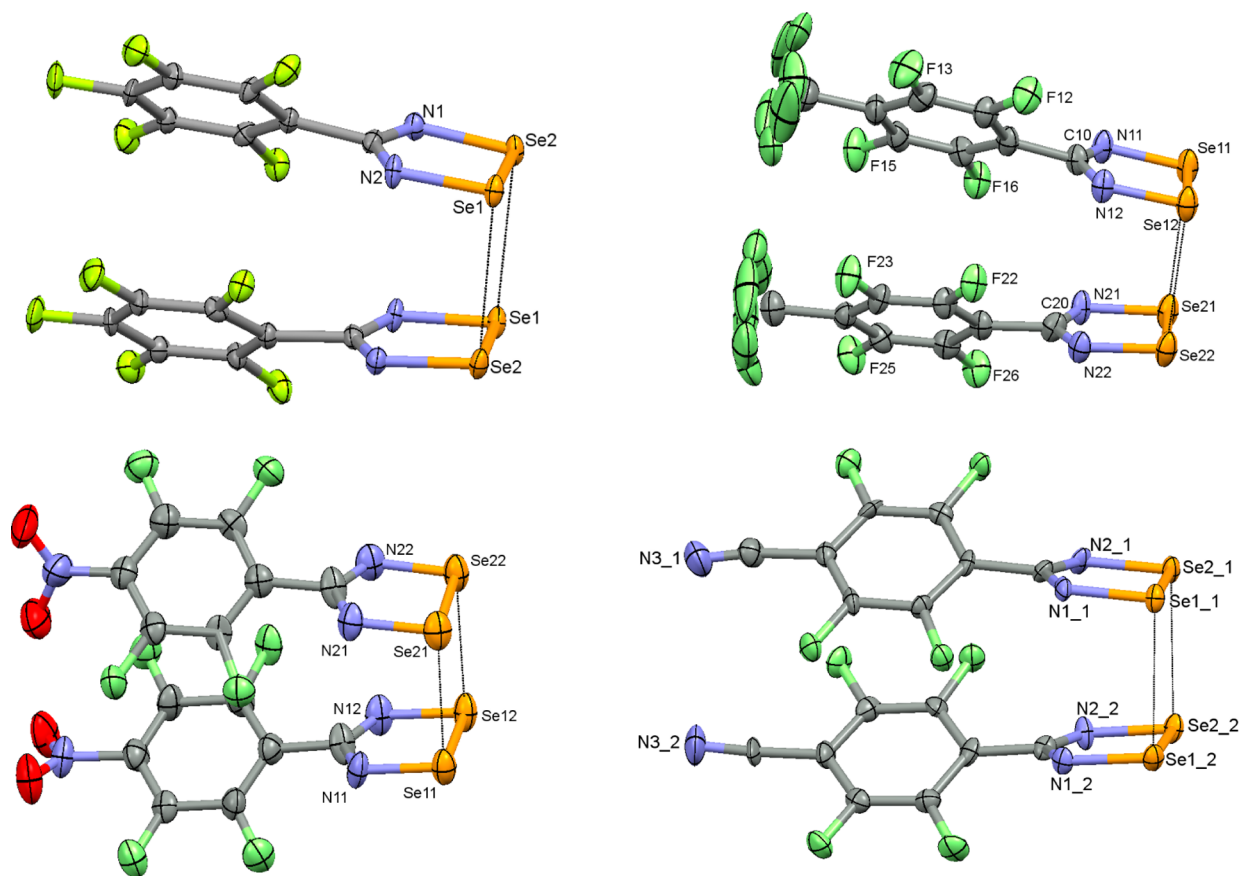


Figure 3. Cisoid dimers formed for (top) **2a** and **2d** and (bottom) **2e** and **2f**.

Both **2a** and **2d** are isomorphous with their DTDA analogues,^{9,30} but the structures of **2e** and **2f** adopt the cisoid dimer conformation, whereas their DTDA analogues are monomeric. However, **2f** is very similar to the nonfluorinated DTDA and DSDA derivatives $p\text{-NCC}_6\text{H}_4\text{CNEEN}$)₂ [$Z' = 2$ with a similar triclinic cell (see the SI)],^{14c} reflecting the

presence of similar structure-directing interactions in all three cases.

A more careful examination of the structures of **2e** and **2f** was therefore undertaken to evaluate why their DTDA congeners disfavored $\pi^*-\pi^*$ dimerization. For **2f**, the most marked component of the structure is the significant “bowing” of the molecular structure, which is observed for both molecules in

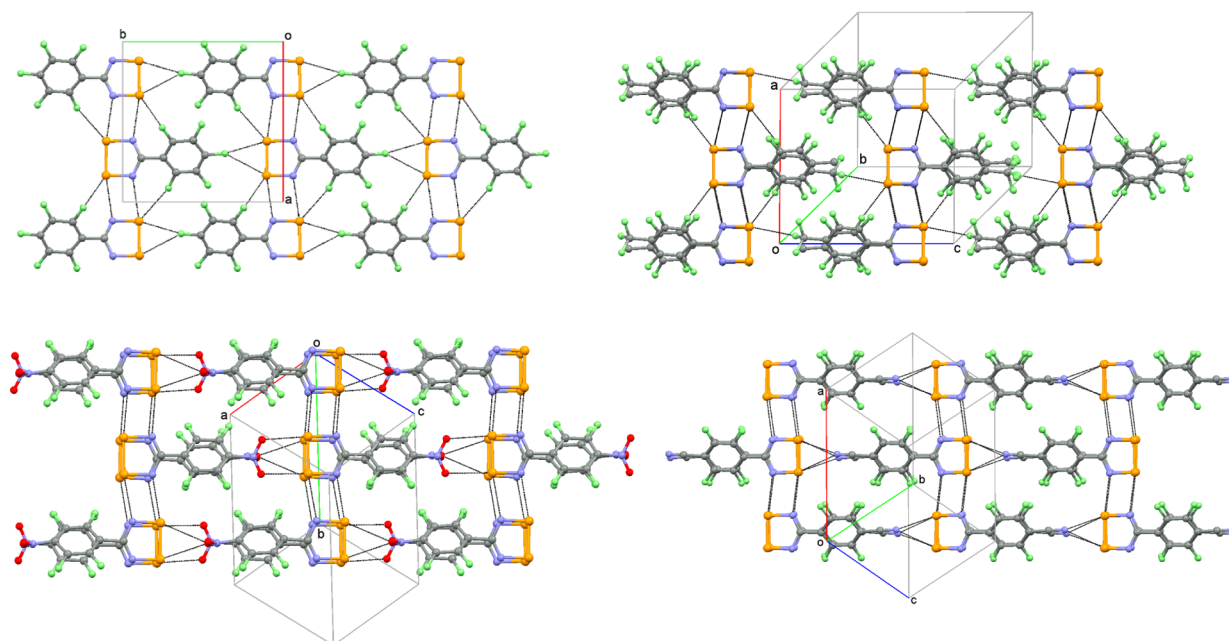


Figure 4. Cisoid dimers formed for (top) **2a** and **2b** and (bottom) **2e** and **2f**.

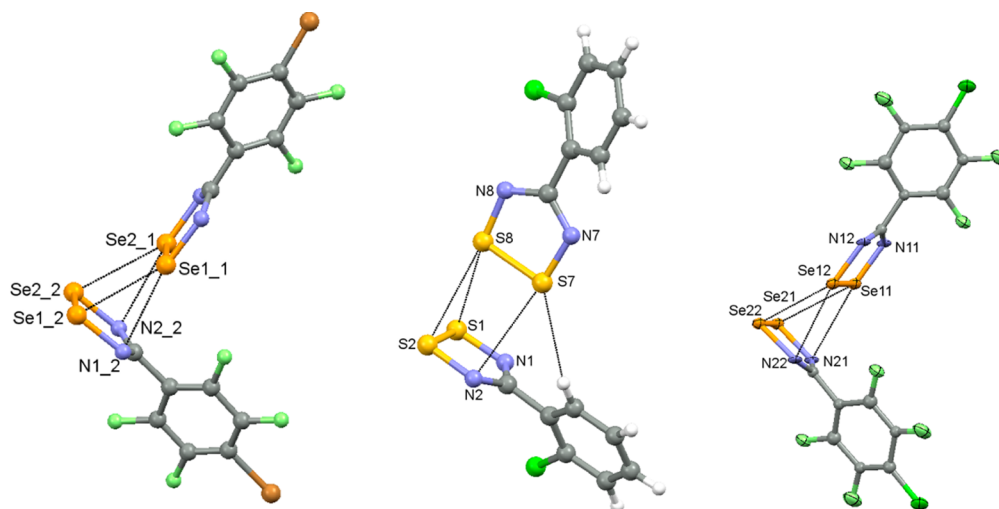


Figure 5. Molecular structures of the dimer **2c** (left), the related orthogonal DTDA dimer (*o*-ClC₆H₄CN₂SSN)₂ (center), and the dimer **2b** (right).

the asymmetric unit with β values of 175.5° . In addition, the C–C≡N bond angles (172.10 and 176.24°) add further to this molecular distortion (Figure 3). The origin of this distortion would appear to derive from (i) the propensity for dimerization through short Se⋯Se intradimer contacts coupled with (ii) the thermodynamic drive to form “in-plane” CN⋯Se interactions. The inclination of the two DSeDA rings (8.96°) therefore requires significant molecular “bowing” to position the cyano groups in an appropriate position to optimize the intermolecular CN⋯Se contacts. Seemingly, both $\pi^*-\pi^*$ dimerization and CN⋯S motifs are structure-directing, and in **2f**, strain is built up within the molecule in order to accommodate both sets of intermolecular contacts. Conversely, in *p*-NCC₆F₄CN₂SSN, the molecular strain is released ($\beta = 180^\circ$) at the expense of $\pi^*-\pi^*$ dimerization, confirming that dimerization is weaker for DTDA radicals than DSeDA radicals and suggesting that the structure-directing CN⋯S interactions (which are retained) are stronger than the dimerization enthalpy (which is lost). In **2e**,

the propensity for dimerization and formation of structure-directing intermolecular Se⋯O contacts is accommodated by a build-up of strain in **2e**, with one molecule exhibiting significant bowing ($\beta = 173.6^\circ$), the largest β value within this series, whereas the DTDA analogue once again releases the molecular strain ($\beta = 180^\circ$) at the expense of dimerization.

All four structures comprise layerlike packing motifs rather than herringbone patterns, which can be understood in terms of the electron-withdrawing nature of the F atoms, which depletes the π -electron density of the aryl ring.⁹ This reduces the strength of Se δ^+ ⋯ π interactions, which typically favor herringbone motifs. The packing of these cisoid dimers adopt chainlike supramolecular structures that support favorable dipole–dipole interactions, and it is worth noting that all four molecules have computed dipole moments in excess of 3.4 D (vide infra), larger than those computed for **2b**, **2c**, and **2g**. “In-plane” CN⋯Se interactions [$3.04(1)$ – $3.14(1)$ Å; Figure 4] in **2f** are reminiscent of the CN⋯S contacts in cyano-

functionalized DTDA radicals⁶ and have also previously been recognized as structure-directing in cyano-functionalized DSeDA radicals.^{26b} In **2f**, the close intermolecular Se \cdots O contacts [2.93(2) – 3.29(2) Å] are comparable to the chain-forming S \cdots O contacts in *p*-O₂NC₆F₄CN₂SSN [S \cdots O 3.228(2) Å].² Molecular electrostatic potential (MEPs) maps (vide infra) indicate that head-to-tail alignment is the most favorable electrostatic term for **2e** and **2f** but not for **2a** and **2d**. Thus, although **2a** and **2d**–**2f** exhibit similar packing motifs, chain formation is most strongly favored through both dipole–dipole and electrostatic contributions in **2e** and **2f**.

Interchain Se $\delta^+\cdots$ N δ^- contacts occur between these chains in all four compounds and are reminiscent of structure-directing “SN-II interactions” described previously by Haynes et al. for the corresponding DTDA radicals.²⁸ These contacts align neighboring chains antiparallel (Figure 4). Despite the larger van der Waals radius of the Se atom,²⁹ the Se \cdots N contacts are significantly shorter (0.15 Å) than the corresponding S \cdots N contacts (Table 4); e.g., **2a** has Se \cdots N contacts of 3.092(6) and 3.097 Å, whereas the corresponding S \cdots N contacts in isomorphous (C₆F₅CN₂SSN)₂ are 3.249(1) and 3.258(1) Å.⁹ This suggests that these contacts play an important and potentially more significant structure-directing role than those within the corresponding DTDA series.

Crystal Structures of (*p*-ClC₆F₄CNSeSeN)₂ (2b**) and (*p*-BrC₆F₄CNSeSeN)₂ (**2c**).** The structures of both **2b** and **2c** comprise unusual dimers in which the two radicals do not associate through conventional face-to-face dimer motifs but adopt an orthogonal geometry that affords a $\pi^*-\pi^*$ -bonding interaction between radicals (Figure 5). Radical **2b** crystallizes in the orthorhombic space group *Pca*2₁ with two molecules in the asymmetric unit, whereas **2c** adopts the monoclinic space group *P*2₁/*c* but also with two molecules in the asymmetric unit. The twist angles between DSeDA and the phenylene ring planes (Table 2) in these orthogonal dimers (56.34–59.70°) are much larger than those in the cisoid dimers (34.65–42.03°) and closer to the energy minimum (ca. 50°). The bowing parameters (β) in these two structures deviate by less than 3° from the idealized 180°. Both the θ and β parameters therefore suggest the release of molecular strain with respect to the cisoid dimers **2a** and **2d**–**2f** such that any potential weakening of the $\pi^*-\pi^*$ dimerization accompanied by a change from cisoid to orthogonal dimerization mode is offset by the release of strain. The “orthogonal” $\pi^*-\pi^*$ interaction in **2b** has the two DSeDA rings inclined at 81.51°, whereas for **2c**, the angle is 84.36°. The intradimer Se \cdots Se [3.110(7)–3.207(7) Å] and Se \cdots N [3.04(3)–3.11(3) Å] contacts within these dimers provide a sufficiently close approach to quenching the radical paramagnetism (vide infra). Such behavior is not entirely without precedent, and in DTDA chemistry, one of the two crystallographically independent dimers within the structure of (*o*-ClC₆H₄CN₂SSN)₂ adopts a similar “orthogonal” $\pi^*-\pi^*$ interaction (Figure 5b), although the relative orientations of the two rings are different.³¹

The packing motifs of **2b** and **2c** are similar to those of orthogonal dimers linked together via additional interdimer Se \cdots N contacts [3.02(2)–3.25(3) Å; Figure 6] to form supramolecular chains. These interdimer contacts are similar to the bifurcated SN-I contacts previously identified in DTDA chemistry. Again it is worth noting that the dimeric structure of **2c** is in contrast to the monomeric *p*-BrC₆F₄CN₂SSN,^{17a} yet in both cases, the electronegative N atom appears to favor contacts to soft, polarizable elements. In **2c**, the orthogonal

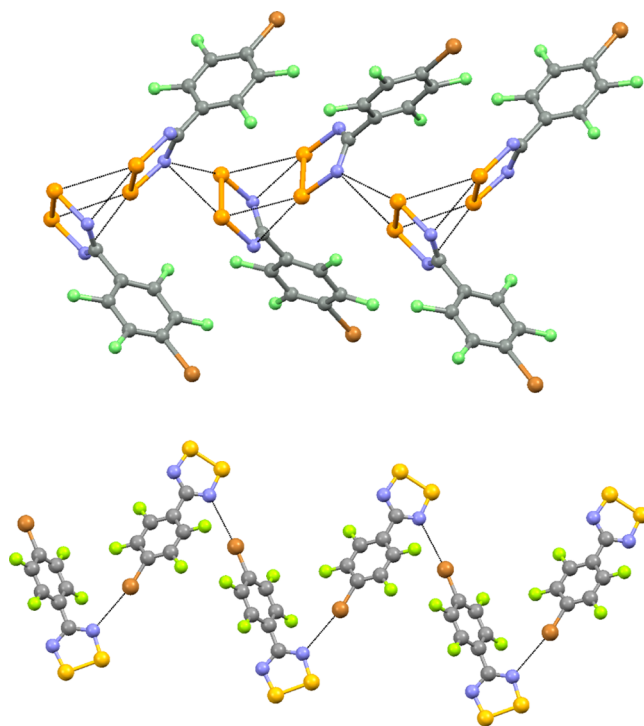


Figure 6. Chainlike motif generated through bifurcated Se \cdots N contacts between orthogonal dimers in **2c** (top) and chainlike motif generated through Br \cdots N contacts within *p*-BrC₆F₄CN₂SSN (bottom).

dimer exhibits close intermolecular bifurcated N \cdots Se contacts, whereas for *p*-BrC₆F₄CN₂SSN, the heterocyclic N atom forms close intermolecular N \cdots Br contacts (cf. the electronegativities of the Se and Br atoms at 2.55 and 2.96, respectively).

Crystal Structure of [2,4,6-(F₃C)₃C₆H₂CNSeSeN]₂ (2g**).** In a “final” attempt to suppress dimerization, the RC₆F₄ substituent was replaced by the sterically demanding perfluoromesityl group 2,4,6-(F₃C)₃C₆H₂. This group has been shown to inhibit dimerization in DTDA radicals, although (F₃C)₃C₆H₂CN₂SSN has been found to be polymorphic, with one phase comprising just DTDA radical monomers and the other phase exhibiting a mixture of both monomers and trans-antarafacial dimers [S \cdots S = 3.443(2) Å].^{17c} Despite the long intradimer S \cdots S separation, SQUID magnetic measurements indicated that below 275 K the trans-antarafacial dimer did not contribute to sample paramagnetism. Radical **2g** crystallizes in the triclinic space group *P* $\bar{1}$ with three molecules in the asymmetric unit, comprising one and a half trans-antarafacial dimers, with the one dimer in a general position and the second dimer located about the crystallographic inversion center associated with the *P* $\bar{1}$ space group. The presence of the two CF₃ groups in the 2 and 6 positions leads to significantly larger twist angles between the aryl and DSeDA ring planes (75.83–89.70°), and the β values (Table 2) reflect negligible geometric strain. The intradimer Se \cdots Se distances of 3.230(2)–3.334(2) Å are markedly shorter than those observed for the sulfur analogue, reflecting a singlet ground state, and closer to the other trans-antarafacial diamagnetic DTDA $\pi^*-\pi^*$ dimer [*m*-NCC₆H₄CN₂SSN)₂; 3.1413(8) Å].^{14c} These trans-antarafacial dimers are linked via interdimer Se \cdots N contacts (Figure 7), which fall in the range 2.840(9)–3.288(9) Å, and comprise both SN-II- and SN-III-like contacts in relation to the established close contacts in DTDA chemistry.¹⁷

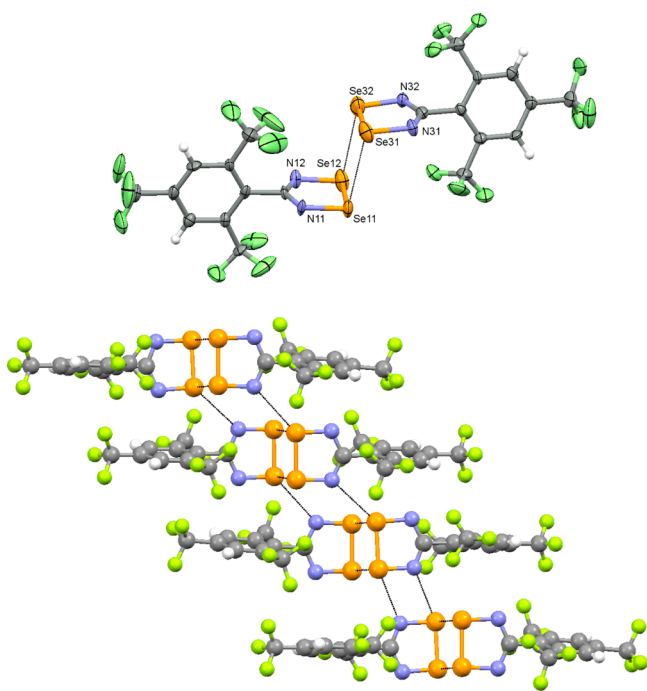


Figure 7. Molecular structure of one of the trans-antafacial dimers of **2g** (top) and solid-state packing of **2g** (bottom), illustrating interdimer Se...N contacts.

Magnetic Studies. The Se...Se contacts within the cisoid dimers **2a** and **2d–2f** as well as the trans-antafacial dimer **2g** are systematically 0.1–0.2 Å longer than those of the cisoid and trans-antafacial DTDA dimers. The increased spin density at selenium and larger radial distribution function, which favors strong dimerization, did not merit SQUID magnetic measurements on these derivatives. In contrast, the unique orthogonal dimerization associated with **2b** and **2c** prompted us to probe their magnetic behavior through SQUID magnetometry. Variable-temperature measurements were made on **2b** and **2c** from 1.8 to 300 K in an applied field of 1 T. Additional M versus H measurements were undertaken at 1.8 and 3.0 K for both **2b** and **2c** in fields of up to 5 T. An additional M versus H plot was recorded for **2c** at 300 K. Both samples were found to be weakly paramagnetic, consistent with singlet dimer configurations and a small number of lattice defects (0.5% monomer with a Weiss constant of -0.6 K in both cases; see the SI). Unlike selected DTDA dimers that exhibit a small increase in paramagnetism upon warming, **2b** and **2c** showed no evidence for an increase in susceptibility up to 300 K, consistent with a well-isolated singlet ground state.

Computational Studies. Previous computational studies on the parent diselenadiazolyl, HCNSeSeN, revealed that valence minimal basis sets were unable to reproduce accurately the molecular geometry, but basis sets implementing effective core potentials supplemented by additional polarization functions were better able to reproduce the bonding within and between diselenadiazolyl radicals.³² More recent computational studies on the dimerization within (HCNEEN)₂ ($E = S, Se$) have shown that successful reproduction of the geometry of these pancake dimers is sensitive to the functional employed;¹² Kertesz et al. identified that some functionals underestimated the intradimer separation, whereas others overestimated this parameter or failed entirely to identify a minimum on the potential energy surface for the weakly bound $\pi^*-\pi^*$ dimer.

The common functional B3LYP, for example, failed to identify the $\pi^*-\pi^*$ dimer as a minimum on the potential energy surface.¹² Their calculations suggested unrestricted M06, BP86, and B97-D3, and the M06-D3 functional appeared to be best suited to reproduce the molecular geometry of the (HCNSeSeN)₂ dimer, successfully locating energy minima in the vicinity of the experimental value. In addition, they examined the convergence of the basis set and found a reasonable energy convergence with a polarized triple- ζ basis set augmented with diffuse functions [6-311++G(d,p)].

We re-examined the M06 functional, which is well-suited for thermodynamic calculations on main-group compounds,³³ along with the PBE0 functional, which reproduces well weak intermolecular forces.³³ All calculations additionally employed Grimme's D3 a posteriori correction for dispersion forces that are not implicitly computed in DFT and that are likely significant for such weak intermolecular interactions.³⁵ In order to improve the computational efficiency for larger structures, we also examined a series of basis sets with effective core potentials in order to reduce the computational burden. Among those we examined, we found that the cc-PVTZ-PP(-F)++ basis set provided very good agreement with the "all-electron" 6-311++G(d,p) used previously,¹² in terms of both the computed geometry and dimerization energy for cisoid (HCNSeSeN)₂.

A subsequent comparison of the M06-D3 and PBE0-D3 functionals (Table 3) led to an excellent reproduction of the

Table 3. Experimental and Computed Distances within the Cisoid Dimer (HCNSeSeN)₂ Using UM06-D3 and PBE0-D3 Functionals^a

	exptl	computed		
		UM06-D3 ²⁶ 6-311++G(d,p)	UM06-D3 cc-PVTZ-PP(-F)++	PBE0-D3 cc-PVTZ-PP(-F)++
Se–Se	2.33	2.35	2.36	2.35
Se–N	1.80	1.77	1.78	1.79
N–C	1.33	1.33	1.32	1.32
Se...Se	3.26	3.14	3.29	3.21
N...N	3.27	3.18	3.25	3.27
C...C	3.31	3.20	3.25	3.29
D_e /(kJ mol ⁻¹)		15	17	21

^aThe dissociation energy D_e is the energy change $E_{\text{dimer}} \rightarrow 2E_{\text{monomer}}$

dimer geometry and a slight increase in the dissociation energy (21 kJ mol⁻¹). At the same level of theory, the dissociation energy of (HCNSeSeN)₂ was computed to be 7 kJ mol⁻¹, indicating that the (HCNSeSeN)₂ dimer is significantly more stable than (HCNSeSeN)₂. Although there is no experimental data on the stability of (HCNSeSeN)₂ itself, the dimerization enthalpies for several DTDA radicals have been measured in solution, e.g., (PhCNSSN)₂ (-37 kJ mol⁻¹), F₃CNSSN)₂ (-37 kJ mol⁻¹), (t-BuCNSSN)₂ (-31 kJ mol⁻¹), and (pyCNSSN)₂ (-35 kJ mol⁻¹).^{23,24} Magnetic measurements on a number of weakly dimerized DTDA radicals^{10,11} have shown the onset of paramagnetism at elevated temperatures from which estimated solid-state dimerization energies in the region of -8 to -11 kJ mol⁻¹ were determined. It is unsurprising that solution and solid-state dimerization enthalpies differ due to variation between the intermolecular forces in the solid-state and solvation effects in solution state. These experimental data are ca. 1–5 times greater than the computed gas-phase value for (HCNSeSeN)₂, placing the

corresponding solution dimerization enthalpy for DSeDA radicals in the 20–100 kJ mol⁻¹ region. Although there is considerable uncertainty in this value, there is no doubt that the experimental and computational data both point to DSeDA radicals exhibiting stronger dimerization enthalpies than the corresponding DTDA radicals.

Dimerization Energy. In order to assess the relative stabilities of the different modes of association for DSeDA dimers, geometry optimizations for (HCNSeSeN)₂ were undertaken for the cis-cofacial dimer, the trans-antarafacial mode of association, and the orthogonal interaction. The optimized geometries are in very good agreement with those determined experimentally. In general, these computations slightly underestimate the closest intradimer contacts, but the agreement overall is remarkably good, with the largest deviation from the experimental data being the Se...Se contact within the trans-antarafacial mode (5% error). The computed dissociation energies indicate that the dimer stability is in the order cis-cofacial > orthogonal > trans-antarafacial (Table 4).

Table 4. Experimental and Computed [PBE0-D3/cc-PVTZ-PP(-F)++] Distances within the Dimer (HCNSeSeN)₂ for Cis-Cofacial, Trans-Antarafacial, and Orthogonal Conformations^a

	cis-cofacial		trans-antarafacial		orthogonal	
	exptl	calcd	exptl	calcd	exptl	calcd
Se–Se	2.33	2.35	2.29	2.34	2.35	2.36
Se–N	1.80	1.79	1.78	1.79	1.80	1.79
N–C	1.33	1.32	1.32	1.32	1.33	1.32
Se...Se	3.26	3.21	3.29	3.16	3.16	3.10
Se...N					3.06	2.96
N...N	3.27	3.27	5.25	5.20	4.85	4.75
C...C	3.31	3.29	6.14	6.22	5.63	5.50
D ₀ / kJ mol ⁻¹		21		16		19

^aThe geometric parameters for trans-antarafacial and orthogonal conformations are averages of those observed experimentally for (RCNSeSeN)₂ dimers.

Previous studies have shown that solid-state molecular geometries cluster near computed energy minima, such that with a statistically significant quantity of data clear correlations exist between the distribution of observed conformations and the energy profile.³⁶ Although the number of DSeDA structures is hardly large for statistical purposes, the computed energies of the different dimerization modes appear to fit well with the experimental observations. A search of the CSD, coupled with the current studies, provides a total of 22 structures for pristine DSeDA radicals, of which 17 (77%) adopt the cisoid conformation and 2 (9%) adopt the orthogonal interaction. Just one example of each of the trans-antarafacial, twisted,³⁷ and trans-cofacial³⁸ dimerization modes (5% each) make up the remainder. Even taking into account the fact that the computed dissociation energies underestimate the experimental data, the modest computed differences between different dimerization modes suggest that other packing forces (dispersion, dipole–dipole, and electrostatic interactions) likely play a significant role in determining the structural outcome of the dimerization process. In order to probe the nature of the intermolecular interactions in derivatives of **2**, in relation to the dimerization energy, we undertook further computations to probe the different contributions to the intermolecular forces.

Dipole–Dipole Interactions. The computed molecular dipoles for radicals **2a–2g** are presented in Table 5. In order

Table 5. Computed [Unrestricted PBE0-D3 cc-PVTZ-PP(-F)++] Dipole Moments for Radicals **2a–2g**

	2a	2b	2c	2d	2e	2f	2g
dipole/D	3.46	4.69	2.96	3.18	6.71	6.20	2.61

to validate these values, we also calculated the dipoles for thiophene (0.54 D) and water (1.86 D) using the same methodology, which were found to be in excellent agreement with experiment.³⁹ It is clear from these data that all radicals in this series exhibit a strong molecular dipole, although the magnitude of the dipole is strongly correlated with the substituent X. At the lower end of the spectrum, **2c** (X = Br) and **2d** (X = Cl) exhibit dipole moments of around 2.5–3.1 D, whereas **2e** (X = CN) and **2f** (X = NO₂) exhibit dipoles in excess of 6 D. It is worth noting that those radicals with a smaller dipole (**2c**, **2d**, and **2g**) do not adopt chain motifs, whereas those with larger dipoles all adopt chainlike structures. When using a point dipole approximation (eq 1),⁴⁰ we find that the large intermolecular distances between centroids along the chain direction give rise to energetically small dipole–dipole interactions. For example, the cyano derivative **2e** has the largest molecular dipole (6.71 D), but the large separation of radicals along the chain direction (12.11 Å) using a point dipole approximation (eq 1) affords a dipole–dipole interaction of ca. 3 kJ mol⁻¹. While this is energetically small in relation to the calculated dimerization energy, it is comparable in relation to the difference in energies between possible dimerization modes.

$$V = (\mu_1\mu_2/4\pi\epsilon_0)(1/d^3)(1 - 3\cos^2\theta) \quad (1)$$

Coulombic Interactions. Electrostatic interactions between DTDA radicals have previously been exploited to account for the possible packing motifs in simple DTDA radicals such as (HCNSeSeN)₂ and (CICNSeSeN)₂.²⁸ The MEPs for **2a–2f**, mapped onto their total electron density surface, are presented in Figure 8. All MEPs reveal regions of positive charge (deep blue) in the vicinity of the Se atoms as the most electropositive area. However, the most electronegative region (red) varies considerably. In **2a** and **2d**, it is clear that the region of largest

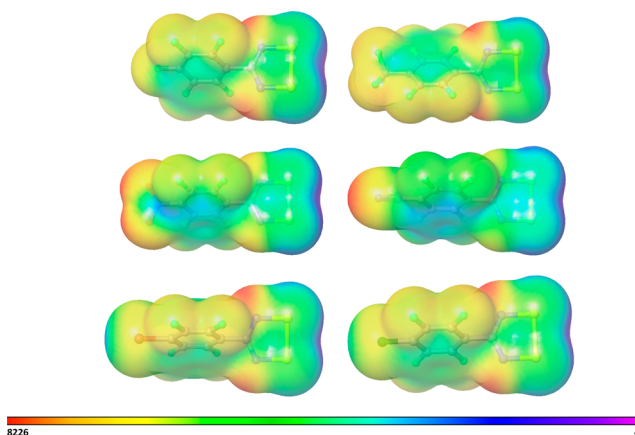


Figure 8. MEPs (atomic units) plotted on the electron density surface for (top) **2a** and **2d**, (center) **2e** and **2f**, and (bottom) **2b** and **2c**. Red represents regions of greatest partial negative charge, and blue-purple represents the largest partial positive charge.

partial negative charge is associated with the heterocyclic N atoms, and thus the most favorable electrostatic interaction is likely to be $\text{Se}^{\delta+}\cdots\text{N}^{\delta-}$. This is manifested in the short lateral contacts perpendicular to the molecular chains [2.941(7)–3.097(6) Å] for **2a** and **2d**. Although the structures of **2e** and **2f** appear superficially similar to **2a** and **2d**, the largest partial charge on the electron density surface now occurs at the cyano and nitro substituents, with a corresponding diminution of negative charge in the vicinity of the heterocyclic N atoms. The strongest electrostatic interaction in these cases would therefore appear to be the $\text{Se}^{\delta+}\cdots\delta^-\text{NC}$ and $\text{Se}^{\delta+}\cdots\text{O}^{\delta-}$ interactions, which generate the experimentally observed molecular chains. The interchain lateral $\text{Se}\cdots\text{N}$ contacts [3.06(3)–3.26(3) Å], while superficially similar to those for **2a** and **2d**, tend to be a little longer on average, presumably as a consequence of the reduction in the partial negative charge at the heterocyclic N atoms. For **2b** and **2c**, the halogen substituents are the most electropositive (green-blue) in the series, and thus the chain-forming $\text{Se}\cdots\text{X}$ ($\text{X} = \text{Cl}, \text{Br}$) interaction is electrostatically unfavorable in relation to $\text{N}\cdots\text{X}$ contacts.

Dispersion. The contribution to dispersion was estimated using the difference in energy between single-point calculations on two molecules of **2f** linked via $\text{CN}\cdots\text{Se}$ interactions (extracted from the solid-state structure) and a single-point calculation on the crystallographically determined geometry of **2f**. The total computed dissociation energy to break the $\text{CN}\cdots\text{Se}$ interaction was 26 kJ mol^{-1} , of which the dispersion (D3) contribution was 5 kJ mol^{-1} .

DISCUSSION

These computational studies indicate that the dimerization energy of DSeDA radicals is ca. 3 times higher than that observed for DTDA radicals, with the cisoid, trans-antarafacial, and orthogonal dimers all appearing as stable entities on the potential energy surface. The cis geometry is most stable and in good agreement with the experimentally determined preference for cisoid solid-state structures. Disruption of this substantial propensity for $\pi^*-\pi^*$ dimerization relies on a series of other competitive noncovalent interactions, which can successfully outcompete the dimerization energy. To date, this has not been achieved in DSeDA chemistry, whereas a number of DTDA radicals do retain their paramagnetism in the solid state. In many cases, the DSeDA and DTDA radicals appear to be isostructural, so the DSeDA analogues of monomeric DTDA radicals provide useful structural comparisons as “hypothetical” dimer conformations. In order to probe these intermolecular interactions, we selected **2f** for further study because both the $\text{CN}\cdots\text{S}$ and $\text{CN}\cdots\text{Se}$ interactions appear as well-established supramolecular synthons. At the PBE0-D3 cc-PVTZ-PP(-F)++ level of theory, the total energy associated with each $\text{CN}\cdots\text{Se}$ interaction is ca. 26 kJ mol^{-1} . With each molecule forming two such interactions (52 kJ mol^{-1}), there is a considerable structural driving force for chain formation. In the DTDA derivative *p*-NCC₆F₄CN₂SSN, dimerization is sacrificed in order to optimize the $\text{CN}\cdots\text{S}$ contacts, whereas in **2f**, the greater dimerization energy inhibits monomer formation, albeit at the expense of some molecular strain. A comparison of the energy of the crystallographically determined structure of **2f** (strained) with its geometry-optimized (unstrained) structure reveals a remarkably large strain energy of ca. 85 kJ mol^{-1} ! Therefore, the driving force for dimerization in **2f** must be clearly substantial, whereas in the lighter sulfur analogue, the strain required to adopt a related cisoid dimer conformation is clearly

too great and dimerization is sacrificed with the release of strain.

CONCLUSION

A number of novel diselenadiazolylys have been prepared and structurally characterized. Four of these derivatives ($\text{X} = \text{F}, \text{CF}_3, \text{NO}_2, \text{CN}$) form cisoid dimers, whereas for $\text{X} = \text{Cl}$ and Br , an unusual orthogonal dimer interaction is adopted. The use of CF_3 groups in the 2 and 6 positions disrupts the preferred cisoid dimer conformation, affording the first example of a trans-antarafacial DSeDA dimer. Computational studies reveal that each of these dimers is a minimum on the potential energy surface, and for the prototypal $(\text{HCNSeSeN})_2$, the order of stability is cisoid > orthogonal > trans-antarafacial, which is in agreement with the observed distribution of structures within the CSD and this current dataset. The propensity for many DTDA and DSeDA radicals to adopt isomorphous structures means that these DSeDA dimers provide valuable alternative hypothetical “dimer structures” for established monomeric DTDA radicals. The observation of dimerization throughout the series **2a–2g** coupled with computational studies reflects stronger dimerization energies for DSeDA radicals in relation to DTDA radicals. This is manifested in significant molecular distortions in the cases of **2e** and **2f** (whose sulfur analogues do not exhibit dimer structures) to accommodate the combination of both favorable dimerization and supramolecular chain-forming interactions. In the DTDA derivatives, dimerization is not observed, but $\text{CN}\cdots\text{S}$ contacts are retained, suggesting that the molecular strain is greater than the dimerization energy gained. A comparison of the strain energy (computed for the selenium analogue **2f**) in relation to the typical dimerization energy in solution for DTDA radicals (35 kJ mol^{-1}) is at least qualitatively consistent with this perspective.

EXPERIMENTAL SECTION

General Considerations. All reactions and manipulations were carried out under an atmosphere of dry, oxygen-free nitrogen using standard double-manifold techniques with a rotary oil pump. A nitrogen-filled glovebox (Saffron Scientific β -range) was used to manipulate solids including storage of starting materials, room temperature reactions, product recovery, and sample preparation for analysis. Molecular sieves (4 Å) were dried at 120 °C for 24 h prior to use. All solvents (diethyl ether, MeCN, toluene, and THF) were dried before use and stored over molecular sieves under a nitrogen atmosphere. Deuterated solvents were dried over molecular sieves before use. Chemicals were purchased from commercial suppliers and used as received or prepared according to the literature methods.⁴¹ SeCl_2 was prepared in situ and used directly by the following method: gray selenium and SeCl_4 were mixed together in a 1:1 ratio in a Schlenk tube without solvent to give SeCl_2 as a dark viscous red-black liquid. An Exeter CE-440 elemental analyzer was used for carbon, hydrogen, and nitrogen elemental analyses. IR spectra were prepared as a Nujol mulls between NaCl plates and recorded on a PerkinElmer Paragon 1000 FT-IR spectrometer. Unit mass spectrometry was performed in positive-ion electron impact mode on a Kratos MS890-EI mass spectrometer.

Synthesis of 2a. Pentafluorobenzonitrile (0.4 mL, 610 mg, 3.16 mmol) was added to a solution of $\text{LiN}(\text{SiMe}_3)_2$ (528 mg, 3.16 mmol) in Et_2O (20 mL) and the solution stirred at room temperature for 16 h. The solution was added via cannula to freshly prepared SeCl_2 (3.17 mmol) at 0 °C. The reaction mixture was allowed to warm to room temperature and stirred for 4 h. The brown precipitate was filtered, washed with Et_2O (3 × 20 mL), and dried in vacuo. Ph_3Sb (882 mg, 2.5 mmol) was added to the crude chloride salt followed by MeCN (20 mL). The reaction mixture was heated to reflux for 5 h and then allowed to cool to room temperature. The solvent was removed in

vacuo and the solid residue purified by sublimation (110 °C, $\sim 10^{-2}$ Torr) with **2a** collected on a water-cooled coldfinger (323 mg, 28%, 0.88 mmol). Elem anal. Calcd for $C_7F_3N_2Se_2$: C, 23.03; H, 0.00; N, 7.67. Found: C, 23.23; H, 0.00; N, 7.51. EI-MS (positive ion): m/z 366.8 (calcd for $[M]^+$: m/z 366.8), 173.8 (calcd for $[NSe_2]^+$: m/z 173.8), 93.9 (calcd for $[NSe]^+$: m/z 93.9), 79.9 (calcd for $[Se]^+$: m/z 79.9), 51.0. IR (ν_{max}/cm^{-1} ; Nujol): 1648(m), 1496(s), 1420(m), 1332(s), 1261(m), 1247(m), 1101(m), 994(s), 958(s), 773(s), 763(m), 703(m), 662(m), 636(m).

Synthesis of 2b. 4-Chlorotetrafluorobenzonitrile (950 mg, 4.53 mmol) was added to a solution of $LiN(SiMe_3)_2$ (760 mg, 4.53 mmol) in Et_2O (50 mL) and the solution stirred for 16 h at room temperature. The resultant solution was added via cannula to freshly prepared $SeCl_2$ (4.53 mmol) at 0 °C. The reaction was allowed to warm to room temperature and stirred for 5 h to yield a brown precipitate, which was filtered, washed with ether (3×20 mL), and dried in vacuo. The crude chloride salt was stirred with silver powder (488 mg, 4.53 mmol) in THF (20 mL) for 18 h, the solvent removed in vacuo, and the crude purple product sublimed (100 °C, 10^{-2} Torr) onto a water-cooled coldfinger to yield **2b** (924 mg, 54%, 2.43 mmol). Elem anal. Calcd for $C_7ClF_4N_2Se_2$: C, 22.04; H, 0.00; N, 7.34. Found: C, 22.39; H, 0.00; N, 7.33. EI-MS (positive ion): m/z 382.8 (calcd for $[M]^+$: m/z 382.8), 209.0 (calcd for $[ClC_6F_4CN]^+$: m/z 209.0), 173.8 (calcd for $[NSe_2]^+$: m/z 173.8), 157.8 (calcd for $[Se_2]^+$: m/z 157.8), 159.8, 143.0, 109.0, 93.9 (calcd for $[NSe]^+$: m/z 93.9), 79.9 (calcd for $[Se]^+$: m/z 79.9), 64.0, 44.0. IR (ν_{max}/cm^{-1} ; Nujol): 1717(m), 1683(m), 1635(m), 1576(m), 1415(m), 1335(m), 1226(w), 976(m), 883(w), 760(m).

Synthesis of *p*-BrC₆F₄CN₂Se₂ (2c). 4-Bromotetrafluorobenzonitrile (1.00 g, 3.94 mmol) was added to a solution of $LiN(SiMe_3)_2$ (836 mg, 5.00 mmol) in Et_2O (50 mL). The mixture was stirred at room temperature for 16 h and the solution transferred via cannula to freshly prepared $SeCl_2$ (5.0 mmol) at 0 °C. The reaction mixture was allowed to warm to room temperature and stirred for 5 h to yield a brown precipitate, which was filtered, washed with ether (3×20 mL), and then dried in vacuo. Half of this crude chloride salt was heated to reflux for 1 h in MeCN (30 mL) with Ph_3Sb (380 mg, 1.08 mmol), the solution cooled to room temperature, and the solvent removed in vacuo, and the resulting purple solid was purified by vacuum sublimation (110 °C, 10^{-2} Torr) onto a water-cooled coldfinger. The process was repeated for the other half of the chloride salt to give **2c** (combined yield: 375 mg, 22%, 0.88 mmol). Elem anal. Calcd for $C_7BrF_4N_2Se_2$: C, 19.74; H, 0.00; N, 6.58. Found: C, 20.20; H, 0.00; N, 6.50. EI-MS (positive ion): m/z 426.1 (calcd for $[M]^+$: m/z 426.8), 371.0, 307.1, 271.0, 154.1. IR (ν_{max}/cm^{-1} ; Nujol): 1633(m), 1406(m), 1334(m), 1261(m), 1218(w), 1095(w), 1018(m), 972(m), 818(w), 752(m), 796(w).

Synthesis of 2d. 4-(Trifluoromethyl)tetrafluorobenzonitrile (243 mg, 1 mmol) was added to a solution of $LiN(SiMe_3)_2$ (167 mg, 1 mmol) in Et_2O (20 mL) to yield a dark-red reaction mixture, which was stirred for 18 h at room temperature. The solution was cooled to 0 °C and added to a freshly prepared sample of $SeCl_2$ (1 mmol). The solution was warmed to room temperature and stirred for 5 h, and the red precipitate was filtered, washed with Et_2O (2×20 mL), and dried in vacuo. The solid was transferred to a two-limbed reaction vessel separated by a grade 3 sinter, and a Zn/Cu couple (33 mg, 0.5 mmol) was added. Liquid SO_2 was condensed onto the mixture and the reaction stirred for 18 h at room temperature. The radical was extracted by repeated washings with SO_2 and then SO_2 removed to yield a purple solid, which was sublimed (10^{-1} Torr, 120 °C) to yield dark crystals of **2d** suitable for X-ray diffraction (20 mg, 5%, 0.05 mmol). EI-MS (positive ion): m/z 417 (calcd for $[M]^+$: m/z 416.8). Elem anal. Calcd for $C_8N_2F_7Se_2$: C, 23.15; H, 0.00; N, 6.75. Found: C, 22.90; H, 0.00; N, 6.68.

Synthesis of 2e. 4-Nitrotetrafluorobenzonitrile (500 mg, 2.27 mmol) was added to a solution of $LiN(SiMe_3)_2$ (380 mg, 2.27 mmol) in Et_2O (40 mL) to form a dark-red solution, which was stirred for 18 h at room temperature. The solution was cooled to 0 °C and added to a freshly prepared sample of $SeCl_2$ (2.27 mmol). The solution was allowed to warm to room temperature and stirred for 5 h. The

resultant red precipitate was filtered, washed with Et_2O (2×20 mL), and dried in vacuo. Silver powder (245 mg, 2.27 mmol) and THF (20 mL) were added to the solid. The solution was stirred at room temperature for 18 h to yield a purple solution. The solvent was removed in vacuo to yield a dark solid, which was sublimed (10^{-2} Torr, 120 °C) to yield dark crystals of **2e** suitable for X-ray diffraction (45 mg, 5%, 0.11 mmol). Elem anal. Calcd for $C_7N_3O_2F_4Se_2$: C, 21.37; H, 0; N, 10.68. Found: C, 21.40; H, 0.14; N, 10.42. EI-MS (positive ion): m/z 394 (calcd for $[M]^+$: m/z 393.8), 348, 237, 207, 174 (calcd for $[NSe_2]^+$: m/z 173.8; calcd for $[C_6F_4CN]^+$: m/z 174.0).

Synthesis of 2f. A solution of $LiN(SiMe_3)_2$ (836 mg, 5.00 mmol) in Et_2O (60 mL) was transferred via cannula to a suspension of tetrafluoroterephthalonitrile (1 g, 5.00 mmol) in Et_2O (15 mL) and the solution stirred at room temperature for 16 h. The solution was then transferred via cannula at 0 °C to freshly prepared $SeCl_2$ (5.0 mmol). The reaction mixture was allowed to warm to room temperature and stirred for 64 h. The brown precipitate was filtered, washed with Et_2O (3×10 mL), and dried in vacuo. Ph_3Sb (558 mg, 1.60 mmol) was added to the crude chloride salt, followed by MeCN (20 mL). The reaction mixture was heated to reflux for 1 h and cooled to room temperature. The solvent was removed under vacuum and the resulting purple solid sublimed (125 °C, 10^{-2} Torr) for 3 h onto a water-cooled coldfinger to yield **2f** (240 mg, 13%, 0.64 mmol). Elem anal. Calcd for $C_8F_4N_2Se_2$: C, 25.83; H, 0.00; N, 11.30. Found: C, 26.38; H, 0.19; N, 10.90. EI-MS (positive ion): m/z 373.8 (calcd for $[M]^+$: m/z 373.8), 173.8 (calcd for $[NSe_2]^+$: m/z 173.8), 159.8 (calcd for $[Se_2]^+$: m/z 159.8), 93.9 (calcd for $[NSe]^+$: m/z 93.9), 79.9 (calcd for $[Se]^+$: m/z 79.9). IR (ν/cm^{-1} ; Nujol): 2250(w,CN), 1644(w), 1488(s), 1435(s), 1331(s), 1262(m), 1058(m), 996(s), 926(w), 800(w), 772(m), 762(m), 734(m), 712(w), 685(w), 670(w), 642(w).

Synthesis of 2,4,6-(CF₃)₃C₆H₂CN₂Se₂ (2g). 1,3,5-Tris(trifluoromethyl)benzene (2.82 g, 10 mmol) was added to a solution of $nBuLi$ (6.25 mL of 1.6 M solution in hexanes, 10 mmol) in Et_2O (20 mL) at 0 °C to yield a cloudy yellow solution. This was stirred for 2 h at room temperature, after which time bis(trimethylsilyl)carbodiimide (1.86 g, 10 mmol) was added to yield an orange solution, which was stirred for 2 h. The solvent was removed in vacuo to yield an orange oil. This oil was redissolved in toluene (20 mL), cooled to 0 °C, and added to a freshly prepared sample of $SeCl_2$ (10 mmol). The solution was warmed to room temperature and stirred for 18 h, and the resultant red precipitate was filtered, washed with Et_2O (2×20 mL), and dried in vacuo. The solid was transferred to a two-limbed reaction vessel separated by a grade 3 sinter and a Zn/Cu couple (325 mg, 5 mmol) added. Liquid SO_2 was condensed onto the mixture and the reaction stirred for 18 h at room temperature. The radical was extracted by repeated washings with SO_2 and then SO_2 removed to yield a purple solid, which was then sublimed (10^{-1} Torr, 100 °C) to yield blue crystals of **2g** suitable for X-ray diffraction (20 mg, 0.5%, 0.04 mmol). EI-MS (positive ion): m/z 481 (calcd for $[M]^+$: m/z 480.8), 307 (calcd for $[(CF_3)_3C_6H_2CN]^+$: m/z 307.0), 288 (calcd for $[C_3F_8C_6H_2CN]^+$: m/z 288.0), 238 (calcd for $[(CF_3)_2C_6H_2CN]^+$: m/z 238.0).

X-ray Crystallography. Crystals of **2a–2g** suitable for X-ray diffraction were all grown by slow sublimation under static vacuum (10^{-2} Torr) in glass sublimation tubes. Crystals were coated in paratone oil and mounted on the end of a glass fiber with fluoropolymer. Data for **2a**, **2d**, and **2f** were collected on a Rigaku AFC7R diffractometer equipped with a Mo $K\alpha$ ($\lambda = 0.7107$ Å) rotating-anode source using ψ scans. Data were corrected for absorption using ψ scans.⁴² Data for **2b**, **2e**, and **2g** were collected on a Nonius Kappa CCD diffractometer with a CCD detector using graphite-monochromated Mo $K\alpha$ radiation. Data were collected using COLLECT⁴³ and integrated and reduced using HKL, DENZO, and SCALEPACK.⁴⁴ A multiscan absorption correction was applied using SORTAV.⁴⁵ In all cases, the sample temperature was maintained using an Oxford Cryosystems Cryostream. All structures were solved by direct methods and refined against F^2 using the SHELXTL package.⁴⁶ Unit cell parameters and refinement statistics are presented in the SI. The structure of **2c** has been reported previously.⁴⁷ All new structures

have been deposited with the Cambridge Crystallographic Data Centre (CCDC 1421399–1421404).

Computational Studies. All calculations were undertaken using *Jaguar v8.7*⁴⁸ with surfaces visualized within *Maestro 10.1*.⁴⁹ All calculations employed either unrestricted M06⁵⁰ or PBE0³⁴ functionals and included a dispersion correction using the D3 method of Grimme.⁵¹ The cc-PVTZ-PP(-F)++ basis set,⁵² which comprises a correlation-consistent triple- ζ basis set incorporating both polarization and diffuse functions, was implemented for all calculations. For calculations of the cis-cofacial, trans-antarafacial, and orthogonal modes of association for [HCNSeSeN]₂, full geometry optimization was undertaken, commencing from a structure adapted from the crystallographic data in which the aryl group was replaced by hydrogen within *Mercury*.⁵³ Dipole moments were computed on the gas-phase-optimized geometries of radicals **2a–2g**. The strength of the intermolecular chain-forming CN \cdots Se interactions in **2f** employed single-point calculations on the dimer pair and the isolated radical using the crystallographically determined geometry. TD-DFT calculations were undertaken on the geometry-optimized structure of **2a**, with the 55 lowest-energy transitions covering the spectrum from 650 to 200 nm. Spectra were visualized and compared to experimental data (1×10^{-4} M) within *Maestro*. Transition energies were scaled by a factor of 0.95 to give a best fit to the experimental data, and the experimental line width was optimized to fit the intense transitions at 369 and 433 nm.

■ ASSOCIATED CONTENT

Supporting Information

The Supporting Information is available free of charge on the ACS Publications website at DOI: 10.1021/acs.inorgchem.6b01771.

EPR analysis of the spin-density distribution, summary of crystallographic data, magnetic data for compounds **2b** and **2c**, and a linear fit of the absorbance versus concentration for the peak at 369 nm (PDF)

X-ray crystallographic data in CIF format for **2a** (CIF)

X-ray crystallographic data in CIF format for **2b** (CIF)

X-ray crystallographic data in CIF format for **2d** (CIF)

X-ray crystallographic data in CIF format for **2e** (CIF)

X-ray crystallographic data in CIF format for **2g** (CIF)

■ AUTHOR INFORMATION

Corresponding Authors

*E-mail: MelenR@cardiff.ac.uk.

*E-mail: jmrawson@uwindsor.ca.

Author Contributions

The manuscript was written through contributions from all authors. All authors have given approval to the final version of the manuscript.

Notes

The authors declare no competing financial interest.

■ ACKNOWLEDGMENTS

R.J.L. and C.M.P. thank the University of Cambridge and EPSRC for financial support. R.L.M. thanks the University of Cambridge for a Domestic Research Scholarship. J.M.R. thanks the EPSRC and NSERC Discovery Grant and RTI programs as well as the Canada Research Chairs program for funding. We particularly thank Dr. J. E. Davies for crystallographic data collection and Dr. A. D. Bond (University of Cambridge) for assistance with the crystallographic data. We thank P. Oliete and F. Palacio (Universidad de Zaragoza) for magnetic measurements on **2b** and **2c**.⁴⁷

■ REFERENCES

- Banister, A. J.; Bricklebank, N.; Lavender, I.; Rawson, J. M.; Gregory, C. I.; Tanner, B. K.; Clegg, W.; Elsegood, M. R. J.; Palacio, F. Spontaneous Magnetization in a Sulfur–Nitrogen Radical at 36 K. *Angew. Chem., Int. Ed. Engl.* **1996**, *35*, 2533–2535. (b) Thomson, R. L.; Pask, C. M.; Lloyd, G. O.; Mito, M.; Rawson, J. M. Pressure-Induced Enhancement of Magnetic-Ordering Temperature in an Organic Radical to 70 K: A Magnetostructural Correlation. *Chem. - Eur. J.* **2012**, *18*, 8629–8633. (c) Palacio, F.; Antorrena, G.; Castro, M.; Burriel, R.; Rawson, J. M.; Smith, J. N. B.; Bricklebank, N.; Novoa, J.; Ritter, C. High-Temperature Magnetic Ordering in a New Organic Magnet. *Phys. Rev. Lett.* **1997**, *79*, 2336–2339.
- Alberola, A.; Less, R. J.; Pask, C. M.; Rawson, J. M.; Palacio, F.; Oliete, P.; Paulsen, C.; Yamaguchi, A.; Farley, R. D.; Murphy, D. M. A thiazyl-based organic ferromagnet. *Angew. Chem., Int. Ed.* **2003**, *42*, 4782–4785.
- Cordes, A. W.; Haddon, R. C.; Oakley, R. T. Molecular conductors from neutral heterocyclic π -radicals. *Adv. Mater.* **1994**, *6*, 798–802.
- Vegas, A.; Pérez-Salazar, A.; Banister, A. J.; Hey, R. G. Crystal structure of 4-phenyl-1,2-dithia-3,5-diazole dimer. *J. Chem. Soc., Dalton Trans.* **1980**, 1812–1815.
- Preuss, K. E. Metal-radical coordination complexes of thiazyl and selenazyl ligands. *Coord. Chem. Rev.* **2015**, *289–290*, 49–61.
- Haynes, D. A. Crystal engineering with dithiadiazolyl radicals. *CrystEngComm* **2011**, *13*, 4793–4805.
- Gillespie, R. J.; Kent, J. P.; Sawyer, J. F. Monomeric and dimeric thiodithiazyl cations, $S_3N_2^+$ and $S_6N_4^{2+}$. Preparation and crystal structures of $(S_3N_2)(AsF_6)$, $(S_6N_4)(S_2O_2F)_2$ and $(S_6N_4)(SO_3F)_2$. *Inorg. Chem.* **1981**, *20*, 3784–3799.
- (a) Gleiter, R.; Bartetzko, R.; Hofmann, P. The Structure of Thiodithiazyl Derivatives An Example of an Electron-Rich-Four-Center-Bond. *Z. Naturforsch., B: J. Chem. Sci.* **1980**, *35*, 1166–1170. (b) Gleiter, R.; Haberhauer, G. Long Chalcogen–Chalcogen Bonds in Electron-Rich Two and Four Center Bonds: Combination of π - and σ -Aromaticity to a Three-Dimensional σ/π -Aromaticity. *J. Org. Chem.* **2014**, *79*, 7543–7552.
- Domagala, S.; Kosci, K.; Robinson, S. W.; Haynes, D. A.; Wozniak, K. Dithiadiazolyl Radicals—Structures and Charge Densities of Their Crystals and Co-Crystal. *Cryst. Growth Des.* **2014**, *14*, 4834–4848.
- (a) Decken, A.; Cameron, T. S.; Passmore, J.; Rautiainen, J. M.; Reed, R. W.; Shuvaev, K. V.; Thompson, L. K. Toward a More General Synthetic Route to Paramagnetic Solids Containing RCN SS^+R Radical Cations. A Structure–Property Correlation for RCN SS^+R ($R = F_3C_2, Cl_3C$). *Inorg. Chem.* **2007**, *46*, 7436–7457. (b) Shuvaev, K. V.; Decken, A.; Grein, F.; Abedin, T. S. M.; Thompson, L. K.; Passmore, J. NC-(CF₂)₄-CNSSN containing 1,2,3,5-dithiadiazolyl radical dimer exhibiting triplet excited states at low temperature and thermal hysteresis on melting–solidification: structural, spectroscopic, and magnetic characterization. *Dalton Trans.* **2008**, 4029–4037.
- (11) (a) Constantinides, C. P.; Eisler, D. J.; Alberola, A.; Carter, E.; Murphy, D. M.; Rawson, J. M. Weakening of the $\pi^*-\pi^*$ dimerisation in 1,2,3,5-dithiadiazolyl radicals: structural, EPR, magnetic and computational studies of dichlorophenyl dithiadiazolyls, Cl₂C₆H₃CN SSN . *CrystEngComm* **2014**, *16*, 7298–7312. (b) Beldjoudi, Y.; Haynes, D. A.; Hayward, J. J.; Manning, W. J.; Pratt, D. R.; Rawson, J. M. Preparation and crystal structures of the isomeric series 4-tolyl-1,2,3,5-dithiadiazolyl, (*o*-MeC₆H₄CN SSN)₂, (*m*-MeC₆H₄CN SSN)₂ and (*p*-MeC₆H₄CN SSN)₂. *CrystEngComm* **2013**, *15*, 1107–1113.
- Beneberu, H. Z.; Tian, Y.-H.; Kertesz, M. Bonds or not bonds? Pancake bonding in 1,2,3,5-dithiadiazolyl and 1,2,3,5-diselenadiazolyl radical dimers and their derivatives. *Phys. Chem. Chem. Phys.* **2012**, *14*, 10713–10725.
- Preuss, K. E. Pancake bonds: π -Stacked dimers of organic and light-atom radicals. *Polyhedron* **2014**, *79*, 1–15.
- (14) (a) Cordes, A. W.; Haddon, R. C.; Oakley, R. T.; Schneemeyer, L. F.; Waszczak, J. A.; Young, K. M.; Zimmerman, N. M. Molecular semiconductors from bifunctional dithia- and diselenadiazolyl radicals.

Preparation and solid-state structural and electronic properties of 1,4-[(E₂N₂C)₆H₄(CN₂E₂)] (E = sulfur, selenium). *J. Am. Chem. Soc.* **1991**, *113*, 582–588. (b) Andrews, M. P.; Cordes, A. W.; Douglass, D. C.; Fleming, R. M.; Glarum, S. H.; Haddon, R. C.; Marsh, P.; Oakley, R. T.; Palstra, T. T. M.; Schneemeyer, L. F.; Trucks, G. W.; Tycko, R. R.; Waszczak, J. V.; Warren, W. W.; Young, K. M.; Zimmerman, N. M. One-dimensional stacking of bifunctional dithia- and diselenadiazolyl radicals: preparation and structural and electronic properties of 1,3-[(E₂N₂C)₆H₄(CN₂E₂)] (E = sulfur, selenium). *J. Am. Chem. Soc.* **1991**, *113*, 3559–3568. (c) Cordes, A. W.; Haddon, R. C.; Hicks, R. G.; Oakley, R. T.; Palstra, T. T. M. Preparation and solid-state structures of (cyanophenyl)dithia- and (cyanophenyl)diselenadiazolyl radicals. *Inorg. Chem.* **1992**, *31*, 1802–1808. (d) Cordes, A. W.; Haddon, R. C.; Hicks, R. G.; Kennepohl, D. K.; Oakley, R. T.; Palstra, T. T. M.; Schneemeyer, L. F.; Scott, S. R.; Waszczak, J. V. Preparation and solid-state structural, electronic, and magnetic properties of the 5-cyano-1,3-benzene-bridged bis(1,2,3,5-dithiadiazolyl) and bis(1,2,3,5-diselenadiazolyl) [5-CN-1,3-C₆H₃(CN₂E₂)₂] (E = S, Se). *Chem. Mater.* **1993**, *5*, 820–825.

(15) (a) Winter, S. M.; Hill, S.; Oakley, R. T. Magnetic Ordering and Anisotropy in Heavy Atom Radicals. *J. Am. Chem. Soc.* **2015**, *137*, 3720–3730. (b) Thirunavukkuarasu, K.; Winter, S. M.; Beedle, C. C.; Kovalev, A. E.; Oakley, R. T.; Hill, S. Pressure dependence of the exchange anisotropy in an organic ferromagnet. *Phys. Rev. B: Condens. Matter Mater. Phys.* **2015**, *91*, 014412. (c) Lakin, K.; Leitch, A. A.; Tse, J. S.; Bao, X.; Secco, R. A.; Desgreniers, S.; Ohishi, Y.; Oakley, R. T. A Pressure Induced Structural Dichotomy in Isostructural Bis-1,2,3-thiaselenazolyl Radical Dimers. *Cryst. Growth Des.* **2012**, *12*, 4676–4684. (d) Winter, S. M.; Oakley, R. T.; Kovalev, A. E.; Hill, S. Spin-orbit effects in heavy-atom organic radical ferromagnets. *Phys. Rev. B: Condens. Matter Mater. Phys.* **2012**, *85*, 094430. (e) Winter, S. M.; Datta, S.; Hill, S.; Oakley, R. T. Magnetic Anisotropy in a Heavy Atom Radical Ferromagnet. *J. Am. Chem. Soc.* **2011**, *133*, 8126–8129. (f) Leitch, A. A.; Lakin, K.; Winter, S. M.; Downie, L. E.; Tsuruda, H.; Tse, J. S.; Mito, M.; Desgreniers, S.; Dube, P. A.; Zhang, S.; Liu, Q.; Jin, C.; Ohishi, Y.; Oakley, R. T. From Magnets to Metals: The Response of Tetragonal Bisdiselenazolyl Radicals to Pressure. *J. Am. Chem. Soc.* **2011**, *133*, 6051–6060. (g) Tsuruda, H.; Mito, M.; Deguchi, H.; Takagi, S.; Leitch, A. A.; Lakin, K.; Winter, S. M.; Oakley, R. T. Pressure dependence of Curie temperature in a selenazolyl radical ferromagnet. *Polyhedron* **2011**, *30*, 2997–3000. (h) Mito, M.; Komorida, Y.; Tsuruda, H.; Tse, J. S.; Desgreniers, S.; Ohishi, Y.; Leitch, A. A.; Cvrkalj, K.; Robertson, C. M.; Oakley, R. T. Heavy Atom Ferromagnets under Pressure: Structural Changes and the Magnetic Response. *J. Am. Chem. Soc.* **2009**, *131*, 16012–16013. (i) Leitch, A. A.; Yu, X.; Robertson, C. M.; Secco, R. A.; Tse, J. S.; Oakley, R. T. Isostructural Bis-1,2,3-Thiaselenazolyl Dimers. *Inorg. Chem.* **2009**, *48*, 9874–9882. (j) Leitch, A. A.; Yu, X.; Winter, S. M.; Secco, R. A.; Dube, P. A.; Oakley, R. T. Structure and Property Correlations in Heavy Atom Radical Conductors. *J. Am. Chem. Soc.* **2009**, *131*, 7112–7125. (k) Robertson, C. M.; Leitch, A. A.; Cvrkalj, K.; Myles, D. J. T.; Reed, R. W.; Dube, P. A.; Oakley, R. T. Ferromagnetic Ordering in Bisthiaselenazolyl Radicals: Variations on a Tetragonal Theme. *J. Am. Chem. Soc.* **2008**, *130*, 14791–14801. (l) Robertson, C. M.; Leitch, A. A.; Cvrkalj, K.; Reed, R. W.; Myles, D. J. T.; Dube, P. A.; Oakley, R. T. Enhanced Conductivity and Magnetic Ordering in Isostructural Heavy Atom Radicals. *J. Am. Chem. Soc.* **2008**, *130*, 8414–8425.

(16) Blundell, S. *Magnetism in condensed matter*; Oxford University Press: Oxford, U.K., 2001.

(17) (a) Antorrena, G.; Davies, J. E.; Hartley, M.; Palacio, F.; Rawson, J. M.; Smith, J. N. B.; Steiner, A. A novel paramagnetic dithiadiazolyl radical: Crystal structure and magnetic properties of *p*-BrC₆F₄CN₂SSN[•]. *Chem. Commun.* **1999**, 1393–1394. (b) Alberola, A.; Less, R. J.; Palacio, F.; Pask, C. M.; Rawson, J. M. Synthesis and magnetic properties of the novel dithiadiazolyl radical, *p*-NCC₆F₄C₆F₄CN₂SSN. *Molecules* **2004**, *9*, 771–781. (c) Alberola, A.; Clarke, C. S.; Haynes, D. A.; Pascu, S. I.; Rawson, J. M. Crystal structures and magnetic properties of a sterically encumbered

dithiadiazolyl radical, 2,4,6-(F₃C)₃C₆H₂CN₂SSN[•]. *Chem. Commun.* **2005**, 4726–4727.

(18) Del Bel Belluz, P.; Cordes, A. W.; Kristof, E. M.; Kristof, P. V.; Liblong, S. W.; Oakley, R. T. 1,2,3,5-Diselenadiazolyls as Building Blocks for Molecular Metals. Preparation and Structures of [PhCN₂Se]⁺PF₆⁻ and [PhCN₂Se]₂. *J. Am. Chem. Soc.* **1989**, *111*, 9276–9278.

(19) (a) Boere, R. T. Short contacts of the sulphur atoms of a 1,2,3,5-dithiadiazolyl dimer with triphenylstibine: first cocrystal with an aromatic compound. *CrystEngComm* **2016**, *18*, 2748–2756. (b) Mills, M. B.; Hollingshead, A. G.; Maahs, A. C.; Soldatov, D.; Preuss, K. E. Isomerization of a lanthanide complex using a humming top guest template: a solid-to-solid reaction. *CrystEngComm* **2015**, *17*, 7816–7819.

(20) Awere, E.; Passmore, J.; Preston, K. F.; Sutcliffe, L. H. A comparative electron spin resonance study of the selenothiadiazolyl radicals *cyclo*-Se_{3–n}S_nN₂⁺ (*n* = 0–3). *Can. J. Chem.* **1988**, *66*, 1776–1780.

(21) Fairhurst, S. A.; Sutcliffe, L. H.; Preston, K. F.; Banister, A. J.; Partington, A. S.; Rawson, J. M.; Passmore, J.; Schriver, M. J. Electron spin resonance spectroscopy of CF₃CN₂SSN[•] and C₆F₅CN₂SSN[•] free radicals. *Magn. Reson. Chem.* **1993**, *31*, 1027–1030.

(22) Luzon, J.; Campo, J.; Palacio, F.; McIntyre, G. J.; Rawson, J. M.; Less, R. J.; Pask, C. M.; Alberola, A.; Farley, R. D.; Murphy, D. M.; Goeta, A. E. Spin density studies on *p*-O₂NC₆F₄CN₂SSN: A heavy *p*-block organic ferromagnet. *Phys. Rev. B: Condens. Matter Mater. Phys.* **2010**, *81*, 144429.

(23) (a) Fairhurst, S. A.; Johnson, K. M.; Sutcliffe, L. H.; Preston, K. F.; Banister, A. J.; Hauptman, Z. V.; Passmore, J. Electron spin resonance study of CH₃CN₂SSN[•], C₆H₅CN₂SSN[•], and SNSN^{•+} free radicals. *J. Chem. Soc., Dalton Trans.* **1986**, 1465–1472. (b) Brooks, W. V. F.; Burford, N.; Passmore, J.; Schriver, M. J.; Sutcliffe, L. H. Paramagnetic liquids: the preparation and characterisation of the thermally stable radical Bu¹CNSNS[•] and its quantitative photochemically symmetry allowed rearrangement to a second stable radical Bu¹CN₂SSN[•]. *J. Chem. Soc., Chem. Commun.* **1987**, *0*, 69–71.

(24) Britten, J.; Hearn, N. G. R.; Preuss, K. E.; Richardson, J. F.; Bin-Salamon, S. Mn(II) and Cu(II) Complexes of a Dithiadiazolyl Radical Ligand: Monomer/Dimer Equilibria in Solution. *Inorg. Chem.* **2007**, *46*, 3934–3945.

(25) Davies, J. E.; Less, R. J.; May, I.; Rawson, J. M. Isolation of the first diselenadiazolyl complex, Pd₃[PhCNSeSeN]₂[PPh₃]₄·2PhMe. *New J. Chem.* **1998**, *22*, 763–765.

(26) (a) Cordes, A. W.; Haddon, R. C.; Hicks, R. G.; Oakley, R. T.; Palstra, T. T. M.; Schneemeyer, L. F.; Waszczak, J. V. Polymorphism of 1,3-Phenylene Bis(diselenadiazolyl). Solid-state Structural and Electronic Properties of b-1,3-[(Se₂N₂C)₆H₄(CN₂Se₂)]. *J. Am. Chem. Soc.* **1992**, *114*, 1729–1732. (b) Davis, W. M.; Hicks, R. G.; Oakley, R. T.; Zhao, B.; Taylor, N. J. Solid state intermolecular interactions in cyanofunctionalized diselenadiazolyl dimers. *Can. J. Chem.* **1993**, *71*, 180–185. (c) Beer, L.; Cordes, A. W.; Myles, D. J. T.; Oakley, R. R.; Taylor, N. J. 1,2,3,5-Dithiadiazolyls and 1,2,3,5-diselenadiazolyls; stacking and packing of π -dimers. *CrystEngComm* **2000**, *2*, 109–114. (d) Parvez, M.; Boere, R. T.; Mook, K. H. A Dimer of 4-(4-Methoxyphenyl)-1,2,3,5-diselenadiazole. *Acta Crystallogr., Sect. C: Cryst. Struct. Commun.* **1995**, *51*, 2118. (e) Cordes, A. W.; Glarum, S. H.; Haddon, R. C.; Hallford, R.; Hicks, R. G.; Kennepohl, D. K.; Oakley, R. T.; Palstra, T. T. M.; Scott, S. R. Preparation and solid state characterization of 1,2,3,5-diselenadiazolyl [HCN₂Se][•]. *J. Chem. Soc., Chem. Commun.* **1992**, 1265–1266. (f) Britten, J. F.; Clements, O. P.; Cordes, A. W.; Haddon, R. C.; Oakley, R. T.; Richardson, J. F. Stacking Efficiency of Diselenadiazolyl π -Dimers. Consequences for Electronic Structure and Transport Properties. *Inorg. Chem.* **2001**, *40*, 6820–6824.

(27) Clarke, C. S.; Haynes, D. A.; Smith, J. N. B.; Batsanov, A.; Howard, J. A. K.; Pascu, S. I.; Rawson, J. M. The effect of fluorinated aryl substituents on the crystal structures of 1,2,3,5-dithiadiazolyl radicals. *CrystEngComm* **2010**, *12*, 172–185.

- (28) Bond, A. D.; Haynes, D. A.; Pask, C. M.; Rawson, J. M. Concomitant polymorphs: structural studies on the trimorphic dithiadiazolyl radical, ClCNSSN[•]. *J. Chem. Soc., Dalton Trans.* **2002**, 2522–2531.
- (29) Nyburg, S. C.; Faerman, C. H. A revision of van der Waals atomic radii for molecular crystals: N, O, F, S, Cl, Se, Br and I bonded to carbon. *Acta Crystallogr., Sect. B: Struct. Sci.* **1985**, *41*, 274–279.
- (30) Pask, C. M. Magneto-structural correlations of some novel sulfur-nitrogen radicals. Ph.D. Thesis, University of Cambridge, Cambridge, U.K., 2003.
- (31) Alberola, A.; Carter, E.; Constantinides, C. P.; Eisler, D. J.; Murphy, D. M.; Rawson, J. M. Crystal structures, EPR and magnetic properties of 2-ClC₆H₄CN₂SSN[•] and 2,5-Cl₂C₆H₃CN₂SSN[•]. *Chem. Commun.* **2011**, 47, 2532–2534.
- (32) Cordes, A. W.; Bryan, C. D.; Davis, W. M.; de Laat, R. H.; Glarum, S. H.; Goddard, J. D.; Haddon, R. C.; Hicks, R. G.; Kennepohl, D. K. Prototypal 1,2,3,5-Dithia- and 1,2,3,5-Diselenadiazolyl [HCN₂E₂][•] (E = S, Se): Molecular and Electronic Structures of the Radicals and Their Dimers, by Theory and Experiment. *J. Am. Chem. Soc.* **1993**, *115*, 7232–7239.
- (33) (a) Zhao, Y.; Truhlar, D. G. *Acc. Chem. Res.* **2008**, *41*, 157; *Acc. Chem. Res.* **2008**, *41*, 157–167. (b) Zhao, Y.; Truhlar, D. G. Density Functional for Spectroscopy: No Long-Range Self-Interaction Error, Good Performance for Rydberg and Charge-Transfer States, and Better Performance on Average than B3LYP for Ground States. *J. Phys. Chem. A* **2006**, *110*, 13126–13130.
- (34) Adamo, C.; Barone, V. Toward reliable density functional methods without adjustable parameters: The PBE0 model. *J. Chem. Phys.* **1999**, *110*, 6158–6170.
- (35) Grimme, S. *Wiley Interdisciplinary Reviews: Computational Molecular Science* **2011**, *1*, 211–228.
- (36) Allen, F. H.; Harris, S. E.; Taylor, R. Comparison of conformer distributions in the crystalline state with conformational energies calculated by ab initio techniques. *J. Comput.-Aided Mol. Des.* **1996**, *10*, 247.
- (37) Bryan, C. D.; Cordes, A. W.; Oakley, R. T.; Spence, R. E. v. H. 4,4'-Dimethyl-1,1'-bi(1,2,3,5-diselenadiazole). *Acta Crystallogr., Sect. C: Cryst. Struct. Commun.* **1995**, *51*, 2402–2404.
- (38) Wu, J.; MacDonald, D. J.; Clerac, R.; Jeon, I.-R.; Jennings, M.; Lough, A. J.; Britten, J.; Robertson, C.; Dube, P. A.; Preuss, K. E. Metal Complexes of Bridging Neutral Radical Ligands: pymDTDA and pymDSDA. *Inorg. Chem.* **2012**, *51*, 3827–3839.
- (39) *CRC Handbook of Chemistry and Physics*, 82nd ed.; Lide, D. R., Editor-in-Chief CRC Press: Boca Raton, FL, 2001.
- (40) Atkins, P.; de Paula, J. *Atkins' Physical Chemistry*, 7th ed.; Oxford University Press: New York, 2002.
- (41) (a) Birchall, J. M.; Haszeldine, R. N.; Jones, M. E. Polyfluoroarenes. Part XVII. Some reactions of pentafluorobenzonitrile. *J. Chem. Soc. C* **1971**, 1343–1348. (b) de Pasquale, R. J.; Tamborski, C. Reactions of fluoroaromatic nitriles with sodium pentafluorophenolate. *J. Org. Chem.* **1968**, *33*, 1658–1661.
- (42) North, A. C. T.; Phillips, D. C.; Mathews, F. S. A semi-empirical method of absorption correction. *Acta Crystallogr., Sect. A: Cryst. Phys., Diffraction, Theor. Gen. Crystallogr.* **1968**, *24*, 351–359.
- (43) COLLECT; Nonius BV: Delft, The Netherlands, 1998.
- (44) Otwinowski, Z.; Minor, W. Processing of X-ray Diffraction Data Collected in Oscillation Mode. In *Methods in Enzymology*, Vol. 276: *Macromolecular Crystallography*; Carter, C. W., Sweet, R. M., Eds.; Academic Press: New York, 1997; Part A, pp 307–326.
- (45) Blessing, R. H. An empirical correction for absorption anisotropy. *Acta Crystallogr., Sect. A: Found. Crystallogr.* **1995**, *51*, 33–38.
- (46) SHELXTL; Bruker AXS: Madison, WI, 2015.
- (47) Feeder, N.; Less, R. J.; Rawson, J. M.; Oliete, P.; Palacio, F. An unprecedented mode of association in diselenadiazolyl radicals: crystal structures and magnetic properties of [p-XC₆F₄CNSeSeN]₂ (X = Cl, Br). *Chem. Commun.* **2000**, 2449–2450.
- (48) Jaguar, version 8.7; Schrodinger, Inc.: New York, 2015.
- Bochevarov, A. D.; Harder, E.; Hughes, T. F.; Greenwood, J. R.; Braden, D. A.; Philipp, D. M.; Rinaldo, D.; Halls, M. D.; Zhang, J.; Friesner, R. A. Jaguar: A high-performance quantum chemistry software program with strengths in life and materials sciences. *Int. J. Quantum Chem.* **2013**, *113*, 2110–2142.
- (49) Maestro, version 10.1; Schrodinger LLC: New York, 2015.
- (50) Zhao, Y.; Truhlar, D. G. The M06 suite of density functionals for main group thermochemistry, thermochemical kinetics, non-covalent interactions, excited states, and transition elements: two new functionals and systematic testing of four M06-class functionals and 12 other functionals. *Theor. Chem. Acc.* **2007**, *120*, 215–241.
- (51) Grimme, S.; Antony, J.; Ehrlich, S.; Krieg, H. A consistent and accurate ab initio parametrization of density functional dispersion correction (DFT-D) for the 94 elements H-Pu. *J. Chem. Phys.* **2010**, *132*, 154104.
- (52) Peterson, K. A.; Figgen, D.; Goll, E.; Stoll, H.; Dolg, M. Systematically convergent basis sets with relativistic pseudopotentials. II. Small-core pseudopotentials and correlation consistent basis sets for the post-d group 16–18 elements. *J. Chem. Phys.* **2003**, *119*, 11113.
- (53) Mercury CSD, version 3.3; Build RC5, <http://www.ccdc.cam.ac.uk/mercury/>.